

Analysis of Natural Rock Slope Deformations under Temperature Variation: A Case Study from Japan

A. Mufundirwa *Rock Mechanics Laboratory, Hokkaido University, Sapporo, Japan*

Y. Fujii *Rock Mechanics Laboratory, Hokkaido University, Sapporo, Japan*

N. Kodama *Hakodate National College of Technology, Hakodate, Japan*

J. Kodama *Rock Mechanics Laboratory, Hokkaido University, Sapporo, Japan*

Abstract

To get better insight into the causative agents of rock falls, natural rock slope deformation across fractures predominantly in a chert rock mass was monitored using six surface fracture displacement sensors. And, the deformations arising from thermal stresses were predicted using (5 m × 5 m) two-dimensional (2D) finite element (FE) plane strain analysis coupled with a model for rock mass expansion due to freezing of pore water. A new and simple method to minimize displacement proportional to temperature (due to thermal response of chert rock mass and sensor) was proposed. By applying the method, the corrected displacement, u' , can be well recognized. Under u' , clear rock mass movement, which could be related to fracture growth was observed. In addition, progressive fracture opening and closure were noted. Results from this study indicate insignificant influences of weather conditions on fracture/rock mass movement. Furthermore, under numerical analysis (FE), in the rock mass model (with 1-m deep fracture), tensile stresses that were large enough to induce fracture growth appeared at the fracture tip when temperature lowered. This research suggests that freezing effects on deformation of chert rock mass are insignificant, and we tentatively suggest that thermal fatigue predominantly caused the permanent fracture deformations.

1 Introduction

Unprecedented catastrophic geohazards continue to affect our daily lives, by causing major fatalities, major loss in terms of economics and extensive damage of property. For example, in Japan, greater than 70% of the land is sloping ground, and to some extent fatal accidents have occurred in the past due to large-scale slope collapse onto roads and railways, disrupting transportation and normal daily activities (Saito 1965, 1969, Shiotani 2003). As a result, ensuring the stability of rock slopes is a major priority.

In a broad sense, numerous factors contribute to rock slope destabilization. Nicolson & Hencher (1997) discuss agents of rock slope deterioration, which include physical and chemical processes, e.g., stress release, cycles of wetting and drying, etc (Matsuoka 2008). They suggested that these mechanisms could cause dilation of existing open and incipient discontinuities allowing ingress of water, rock fragments, organic material, and other damaging elements, hence destabilizing rock slopes. More importantly, the presence of fractures could also affect rock mass strength and increase ingress of water thereby causing instability.

In cold regions, cycles of freezing and thawing could cause rock slope instabilities (Matsuoka 2001, 2008, Nicholson & Nicholson 2000). Murton et al. (2006) introduced the concept of rock fracture and crack growth by ice segregation in cold regions. In line with that, Matsuoka (2008) reinforces ice segregation as emanating from long-term slowing freezing.

Thermal effects on rock mass deformation are also a practical concern. Ishiguro & Nakaya (1986) and Waragai (1998) mentioned that the possibility of crack/fracture initiation due to temperature variations must be taken into consideration for structural safety: temperature fluctuations in the rock mass could be caused by external weather

conditions or by heat generation in the sub-surface environment. Therefore, it is essential to understand fracture behaviour under various conditions, especially under temperature changes (Kostak et al. 1998).

In this paper, a 767-day-long displacement and temperature record for a natural rock slope in Iwate prefecture (Shimohei district, Kawai village) in Japan is described (Fig. 1a). Fracture displacement sensors were installed on the surface of a natural rock slope for continuous measurement of rock slope deformations. A new and simple method was proposed to reduce the apparent displacements (masking the true rock mass displacements) so that we could establish more accurate displacements. The thermal behaviours of a rock mass and a rock slope, both with a one-metre deep fracture subjected to temperature variations, were numerically analyzed. Important thermal deformation characteristics were deduced from the field measurements and numerical results.

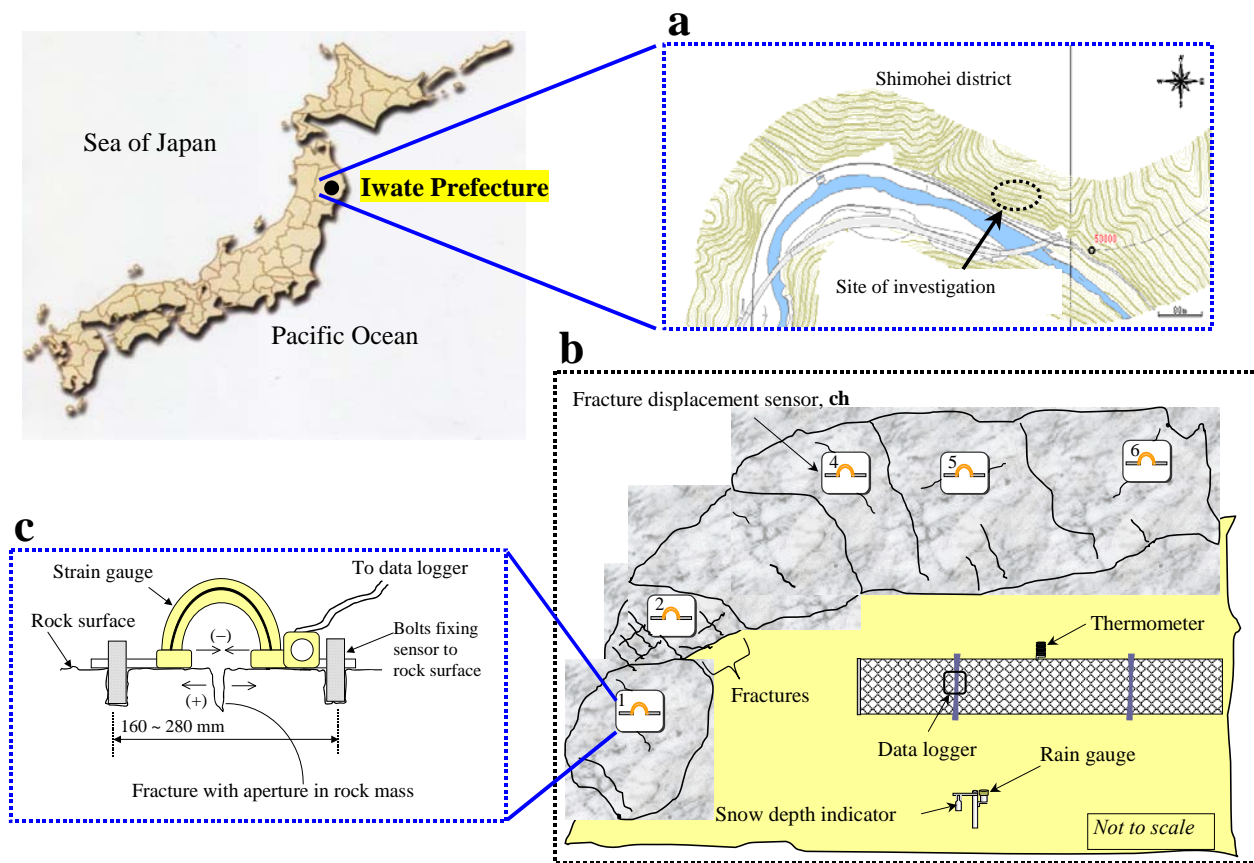


Figure 1. (a) Topographic view for the investigation site, (b) Schematic diagram of natural rock slope showing layout of fracture displacement sensors and meteorological equipments, and (c) Setting of fracture displacement sensor.

2 Site investigation

A field investigation was conducted on a natural rock slope on a south-facing mountain side in Iwate prefecture (Shimohei district, Kawai village) in Japan (Fig. 1a). The topography of the steep rock slope with a dip ($> 65^\circ$) is also shown in Figure 1a. Geologically, the rock slope consists of a chert block with some spatially distributed slates; both rocks are severely jointed within the North Kitakami Belt, the accretionary wedge. This area is located in cool temperate zone, with relatively moderate snowing winter and high humidity most of the time.

Six surface fracture displacement sensors (ch1–ch6) were installed on the surface of natural rock slope as shown in Figures 1b and 2. The fracture displacement sensors (Kyowa, BCD-5B model) had an operating range of -10 to 60 °C, a measuring range of ± 5 mm, and a rated output of ± 1 mV/V (2000×10^{-6}). Weather conditions namely, air temperature, humidity, snowfall, and rainfall were recorded from 9 November 2006 to present. Data through 14 December 2008 were analyzed. Data from all the instruments were recorded automatically at 30-minute intervals using a data logger (CR series, Campbell Scientific).

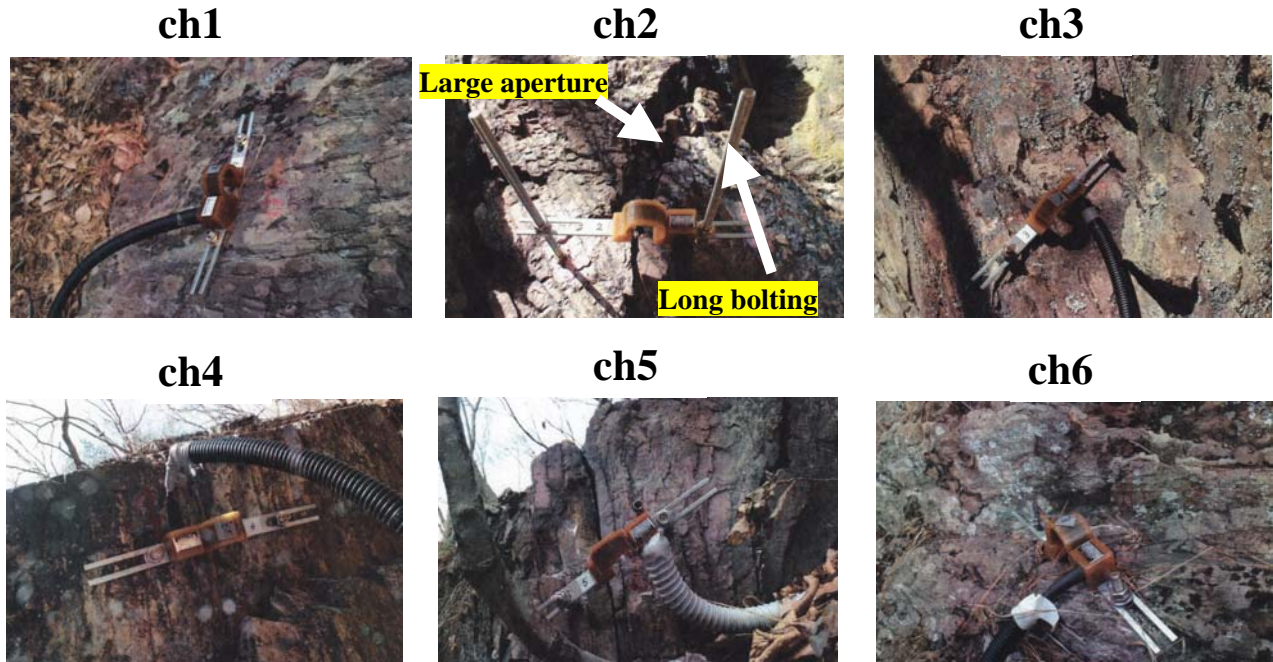


Figure 2. (a) Fracture displacement sensors (ch1–ch6) installed on surface of natural rock slope in Iwate prefecture (Japan).

3 Interpretation of field data

Variations of fracture displacement (u) and air temperature (T_a) for the natural rock slope for each channel are shown in Figure 3. From observation, maximum and minimum temperatures achieved were 23 °C and -4.1 °C, respectively (ch1, Fig. 3). Roughly, temperature-induced displacement varied sinusoidally with temperature, indicating thermal expansion/contraction (all channels, except ch2 in Fig. 3). This means other displacements that occur (e.g., sudden displacement trend changes), may be due to external factors/processes affecting fracture/rock mass movement (Nicolson & Hencher, 1997).

For ch1, in the range $t = 257$ – 286 days, the fracture/rock mass moved (ch1 in Fig. 3). It occurred during the summer period from 23 July 2007 to 21 August 2007. A sharp displacement of 0.2 mm was recorded. This displacement was not temperature-induced as illustrated with ch1 in Figure 4. Furthermore, there was little rain 0 – 2.2 mm/day (see $t = 257$ – 286 days in Fig. 5a) and humidity was generally high ($> 80\%$) as evidenced in Figure 5b. Fracture displacement sensor, ch2, was installed on a highly fractured rock mass (see ch2, Fig. 2). It gave variations of displacement significantly different from all the other channels (ch2 in Fig. 4). Ch2 has a positive slope, whilst the other channels have a negative slope (Fig. 4). The close linear relationship reflected in ch3 and ch5 ($R^2 = 0.98$ and 0.96), shows closeness to elastic (recoverable) deformations (Fig. 4). Ch4 and 6 recorded some permanent deformations of 0.126 mm and 0.187 mm, respectively, from the start (S) to end (E) of monitoring (Fig. 4).

To some extent, the observed displacement data contain displacement components that are proportional to temperature caused by the thermal response of the rock mass, fracture displacement sensors and materials fixing/holding the sensors onto the surface of rock slope. Therefore, attempts to minimize these apparent displacement components were done in order to get the true displacement components due to external processes.

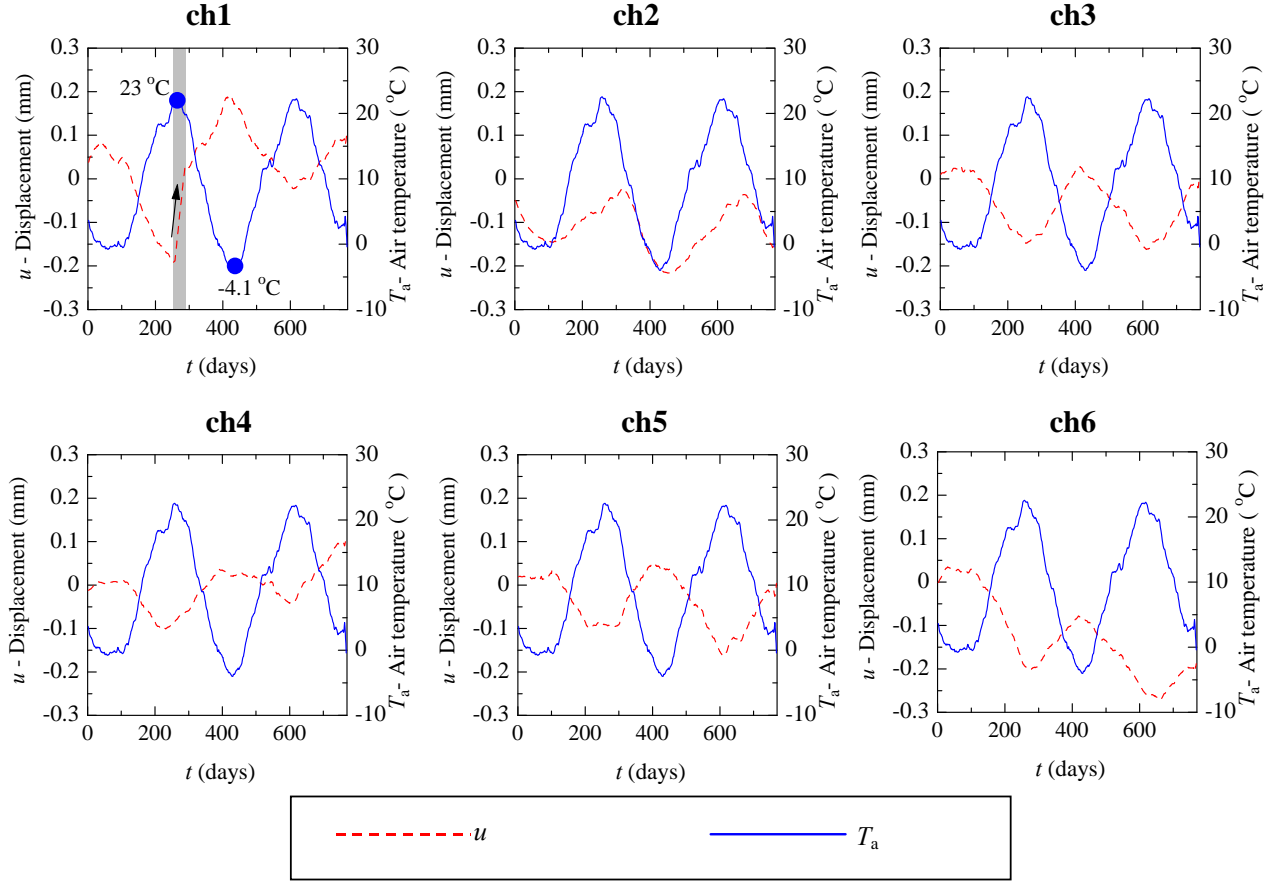


Figure 3. Temporal variations in displacement u (daily average) and air temperature T_a (daily average) for six surface fracture displacement sensors, ch1–ch6. A sharp movement (arrow) occurred at $t = 257$ – 286 days.

4 Corrected displacements

First and foremost, to minimize displacement components that are proportional to temperature, the following equations were used:

$$u' = u + AT_a \quad [1]$$

$$U_a = u'_{\max} - u'_{\min} \quad [2]$$

where u is measured displacement (one-day moving-average), u' is the corrected displacement, A is thermal correction coefficient, T_a is air temperature (one-day moving-average), U_a is displacement amplitude, u'_{\max} is maximum corrected displacement, and u'_{\min} is minimum corrected displacement.

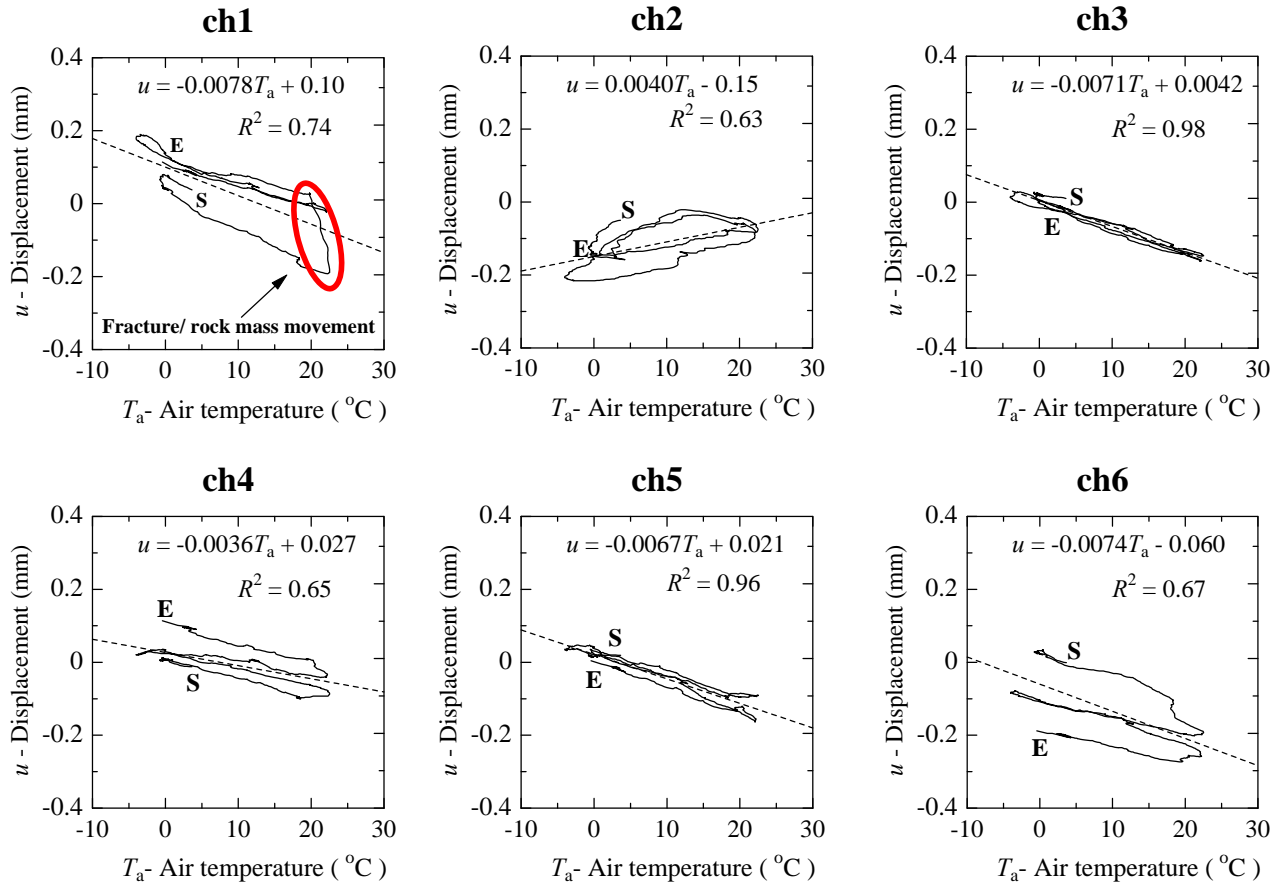


Figure 4. Temporal variations in displacement u (daily average) against air temperature T_a (daily average) for ch1–ch6. Note: **S** and **E** denote the start and end of monitoring.

Different thermal correction coefficients, A , were determined for ch1–ch6. To compute A , an iterative approach was used, which is somewhat time-consuming. Intuitively, the thermal correction coefficient, A , that gave the lowest/minimum displacement amplitude was used to correct the displacement (Fig. 6). In other words, a low A implies minimum temperature effects or erroneous displacements. With reference to Figure 6, A ranges from +0.005 to +0.007 mm/°C, except for ch2. For verification, the displacement sensor was calibrated in the laboratory and $A = +0.00721$ mm/°C was obtained.

At ch2, $A = -0.003$ mm/°C, which is different from other channels (Fig. 6). This may be attributed to the highly fractured nature of the surrounding rock mass within its vicinity (see ch2 in Fig. 2). Setup of the displacement sensor was different from the other channels as shown by the elongated bolt supporting the displacement sensor (ch2 in Fig. 2). This sensor arrangement might have impacted on the real/true rock displacement at ch2. Furthermore, at ch2, fracture tends to open or close with temperature variation with some time lag (ch2 in Fig. 7).

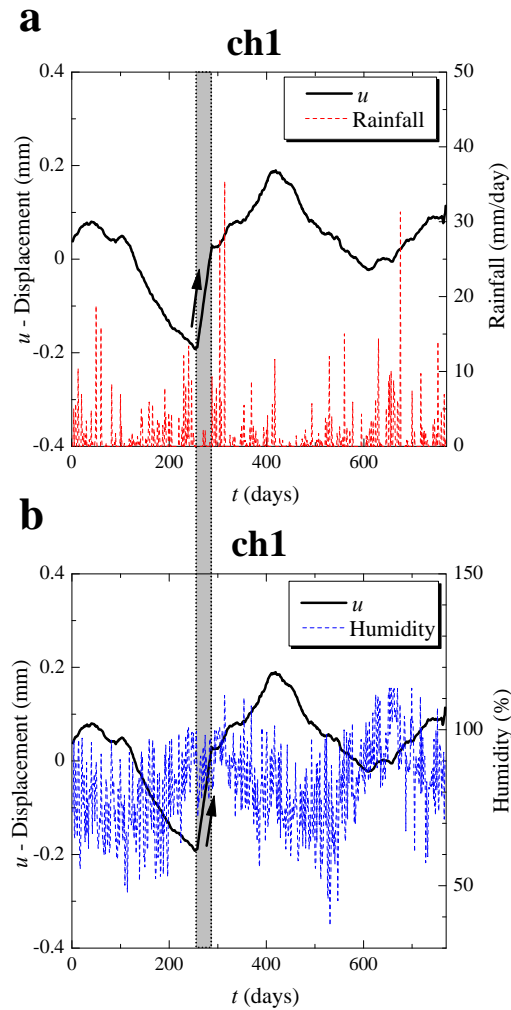


Figure 5. Temporal variations in displacements and meteorological factors for ch1: (a) displacement vs. rainfall, (b) displacement vs. humidity. A sharp movement (arrow) occurred at $t = 257\text{--}286$ days.

Figure 7 shows that displacement variations at ch3 and ch5 are very small, and the possibility of fracture propagation is very low. At ch4, the fracture is gradually opening, and the possibility of fracture propagation is high (ch4 in Fig. 7). This phenomenon may be explained by creep or sub-critical fracture growth (inelastic fatigue) of the rock mass, possibly due to the presence of cyclic thermal stresses at the crack tip. In contrast, at ch6 (Fig. 7), fracture is generally closing possibly due to viscous deformation.

Notably, relations between the corrected displacement and air temperature show near-horizontal patterns/slopes for ch3 and ch5 (Fig. 8); this indicates insignificant rock mass deformations. In principle, abnormal deviations from linearity are considered as fracture/rock mass movement caused by external processes, such as dilation of existing fractures by root growth, freeze-thaw and so forth (ch1 in Fig. 8). Small permanent deformations (0.0014–0.21mm) were observed in all the channels in two years (Fig. 8).

Essentially, after correction at ch1 in Figure 7 (u' using $A = +0.007 \text{ mm}/^\circ\text{C}$), the steep increase in fracture displacement (at $t \approx 36\text{--}40$ weeks) became more apparent than in raw data (ch1 in Fig. 3). As an important feature, it was noted that the computed coefficients (+0.005 to +0.007 $\text{mm}/^\circ\text{C}$) are close to the determined laboratory coefficient (+0.00721 $\text{mm}/^\circ\text{C}$), except for ch2. This means that fractures in chert rock mass have little or insignificant deformations with temperature variation (Fig. 7).

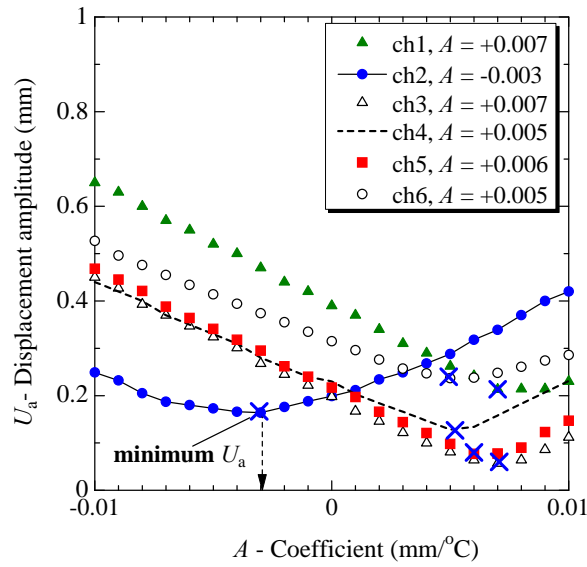


Figure 6. Displacement amplitude U_a vs. thermal correction coefficient A , for six surface fracture displacement sensors, ch1–ch6. Symbol \times , depicts points of minimum temperature effects.

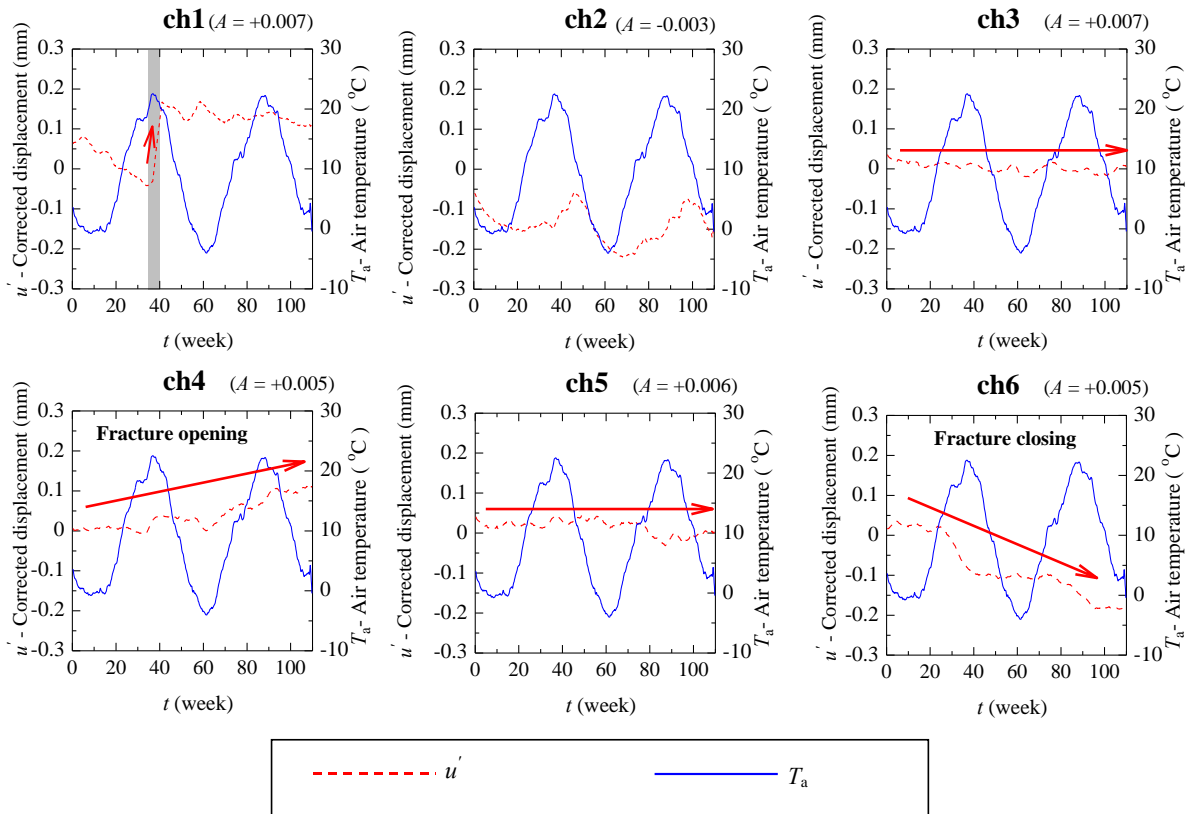


Figure 7. Temporal variations in corrected displacement u' (moving averaged) and air temperature T_a (moving averaged) for ch1–ch6.

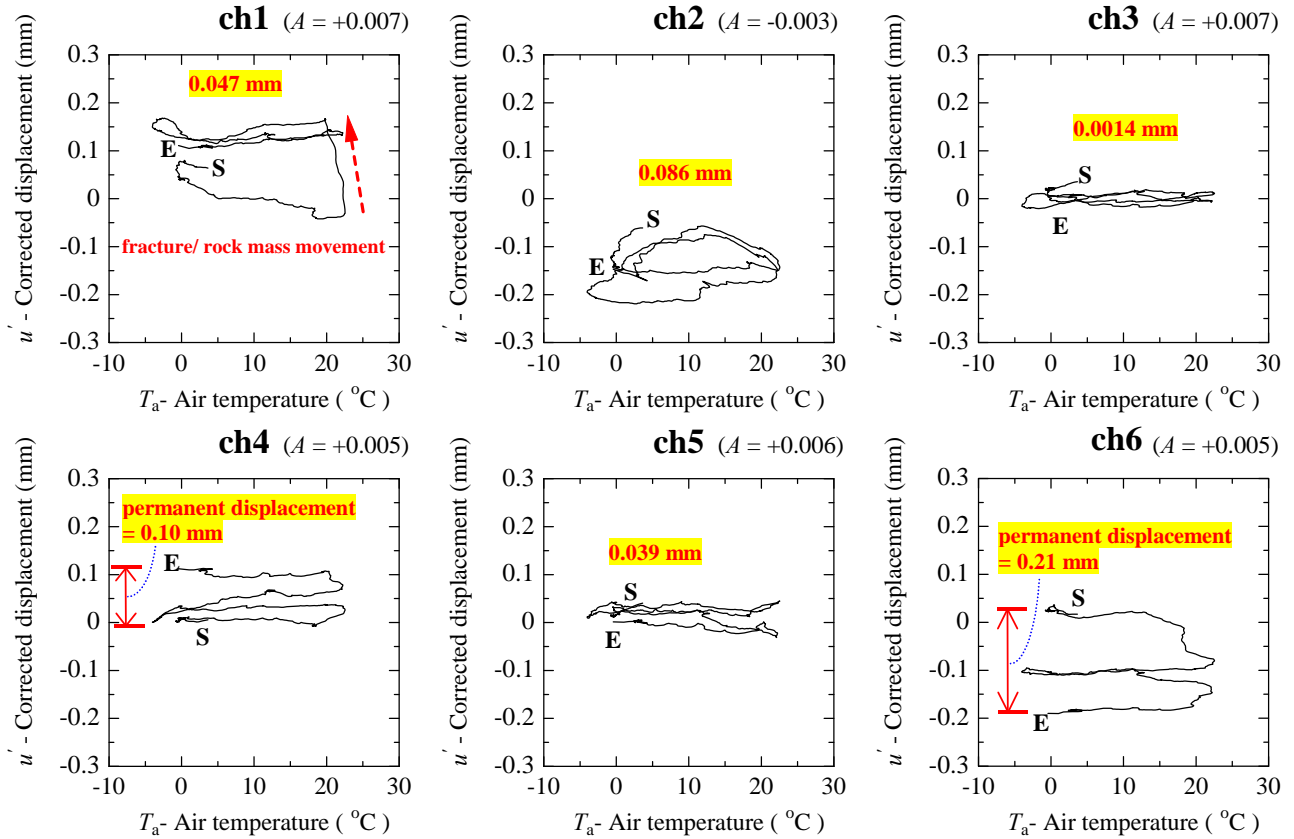


Figure 8. Temporal variations in corrected displacement u' (daily average) and air temperature T_a (daily average) for ch1–ch6. *Note:* S and E denote the start and end of monitoring.

5 Numerical simulation of rock slope deformation

To get a better insight into the deformation of a fracture under temperature variation, numerical analyses for a rock mass with a one-metre deep fracture under temperature variations were carried out using (5 m × 5 m) two-dimensional plane strain analysis coupled with the fundamental heat transfer equation using the Crank-Nicolson method (Crank 1975, William et al. 2007).

Two boundary conditions were used; confined and unconfined conditions to simulate different in-situ conditions under elastic and elasto-plastic finite element analysis as shown in Fig. 9 (Timoshenko & Goodier 1969). To simulate temperature in the field, two patterns of transient heat analysis (variable temperature boundary) were exclusively applied on the top rock surface under confined and unconfined conditions for duration of 52 weeks. The first temperature pattern had a positive temperature variation (7.8–32.2 °C), with an initial rock mass temperature (T_{ref}) of 20 °C applied. The second temperature pattern had positive and sub-zero temperatures (–2.2–22.2 °C), with an initial temperature of 10 °C applied as the temperature of rock mass. With reference to Fig. 10, we defined:

$$\varepsilon = \alpha \Delta T \quad [3]$$

where ε is the thermal strain due to temperature variation, α is the thermal expansion coefficient of rock; ΔT is the change in temperature. It was assumed that rock expands from T_1 to T_2 due to freezing of pore water, where T_1 is the temperature at which freezing starts; T_2 is the temperature at which freezing finishes (Fig. 10).

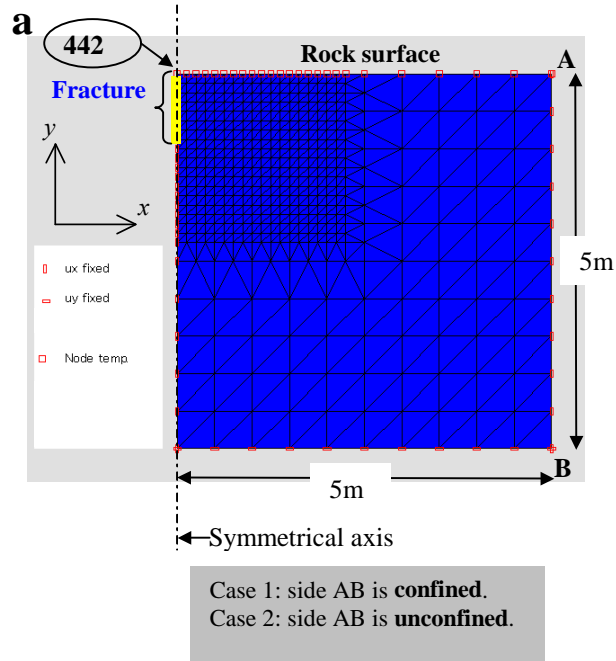


Figure 9. Finite element mesh configuration used in numerical simulation for confined and unconfined boundary conditions: *Note*: 442 is node number that represents the beginning of the fracture at the rock surface. The fracture has some aperture.

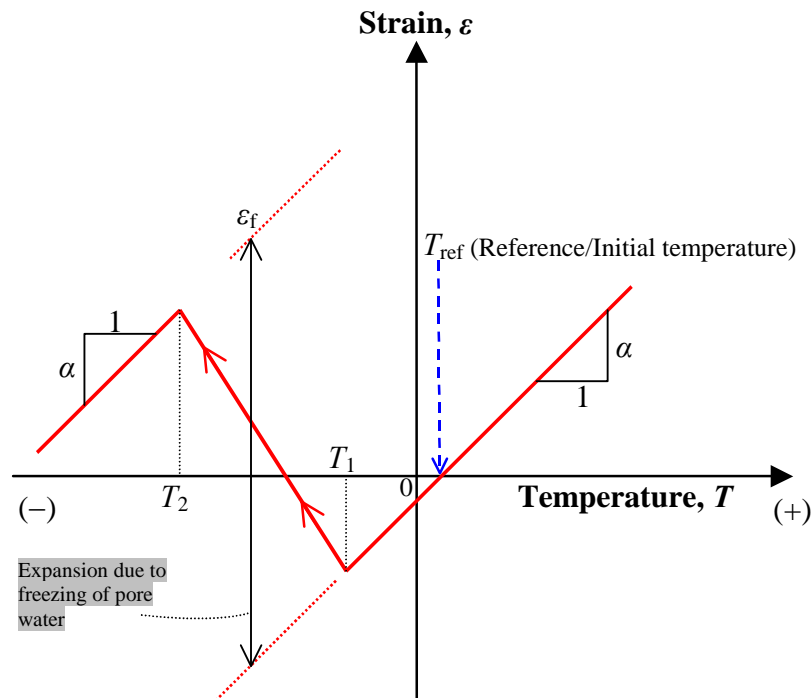


Figure 10. Model for expansion due to freezing of pore water.

5.1 Analytical model and conditions

A two-dimensional finite element mesh was generated (864 triangular elements, 467 nodes). The thermal displacements in the x -direction under elastic analysis (u_x^e) and elasto-plastic analysis (u_x^{ep}) were calculated by considering nodal displacements of the fracture at the rock surface (node 442) as shown in Fig. 9. Stress in the x -direction ($\text{sig}x/\sigma_x$), normal to the fracture axis was mainly considered; it is these stresses that have a high possibility of causing fracture propagation. The model is symmetrical about the y -axis, and tensile stresses are taken as positive (+) whilst compressive stresses as negative (–) in these numerical analyses. Positive displacement means fracture opening and negative displacement means fracture closure (Fig. 1c). A total of 8 numerical simulations were performed; these are elastic and elasto-plastic analyses (confined and unconfined) under the two transient temperature patterns as mentioned above. The rock mass is assumed to be homogeneous and isotropic, and the properties of the rock mass used in the FE analyses are as in Table 1.

Table 1. Properties of rock mass used in numerical model.

Property	Symbol	Value	Formula
Young's modulus	E	110 (GPa) ^m	
Poisson's ratio	ν	0.2 ^a	
Uniaxial compressive strength	σ_c	181 (MPa) ^m	
Angle of internal friction	ϕ	30 ^{oa}	
Friction angle of rupture plane	ϕ'	30 ^{oa}	
Tensile strength (intact)	σ_t	20.4 (MPa) ^m	
Residual tensile strength	σ_t'	0 (MPa) ^a	
Thermal conductivity	K	7.40 (W/ m K) ^m	
Specific heat	c	995 (J/ kg K) ^m	
Density	ρ	2636 (kg/m ³) ^m	
Expansion coefficient	α	7.94×10^{-6} (K ⁻¹) ^a	
Effective porosity	η	0.8% ^m	
Volumetric ice expansion due to freezing	ε_v	9% ^a	
Linear expansive strain due to freezing	ε_i	0.00036 ^a	$\sim(\eta \times \varepsilon_v)/2^*$
Temperature at which freezing starts	T_1	0 °C ^a	
Temperature at which freezing finishes	T_2	–30 °C ^a	

^m measured.

^a assumed.

* 2 is used because of plane strain analysis.

6 Simulation results and discussion

Thermal displacements under elastic (u_x^e) and elasto-plastic conditions (u_x^{ep}) were computed, and the stability of the natural rock mass was then assessed by analysing displacement from the numerical simulations.

6.1 Elastic analysis

Elastic-confined conditions under positive temperature (7.8–32.2 °C) were simulated as shown in Figure 11. As temperature increased, the rock mass expanded, (e.g., at maximum temperature 32.2 °C, there is rock mass expansion) as shown in Figure 11a. Initially, a slight aperture is assumed for the fracture so that the expansion is allowed. Expansion of rock mass across the fracture axis (Fig. 11a) practically means fracture closure. At the fracture tip, compressive stresses were observed, in which stress in the x -direction was less than the uniaxial compressive strength ($-\sigma_x < \sigma_c$); therefore no compressive failure was observed (Fig. 11b). As temperature decreased, the rock mass contracted (e.g., at minimum temperature 7.8 °C, rock mass contracted) as illustrated in Figure 11c, thereby causing the fracture to open. Large tensile stresses around 30.8 MPa, in which stress in the x -direction was greater than the tensile strength of intact rock ($\sigma_x > \sigma_t$) were observed at the fracture tip (Fig. 11d). This condition could lead to fracture propagation, thereby deepening the fracture into the rock mass (Waragai 1998).

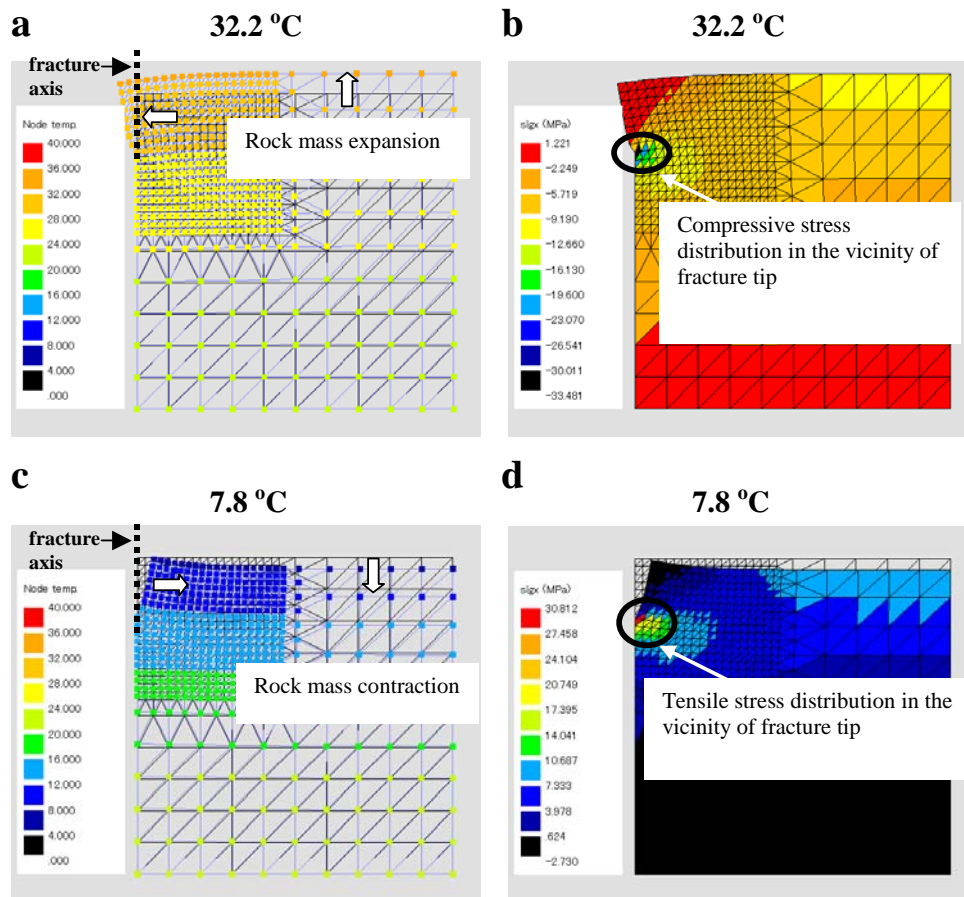


Figure 11. Calculated results of Elastic-confined FE model: (a) Temperature distribution in rock mass at maximum temperature, 32.2 °C, (b) Stress in x -direction (sig_x / σ_x) at 32.2 °C, (c) Temperature distribution in rock mass at minimum temperature, 7.8 °C, and (d) σ_x at 7.8 °C. *Note:* Deformation is magnified $\times 1000$.

Similarly, *elastic-unconfined* conditions within (7.8–32.2 °C) were analyzed. For brevity, it was also found that fracture tends to close and open with temperature increase and decrease, respectively. At minimum temperature of 7.8 °C, small tensile stresses of 13.2 MPa ($\sigma_x < \sigma_t$) appeared at fracture tip (Table 2); therefore fracture propagation is unlikely to occur. In a brief summary, *elastic-confined* conditions within the –2.2 to 22.2 °C temperature range and *elastic-unconfined* conditions within the –2.2 to 22.2 °C temperature range are shown in the Table 2. The maximum tensile stress generated (29.2 MPa) at –2.2 °C is smaller compared to that at minimum temperature of 7.8 °C (30.8 MPa), as shown in Table 2. This is due to expansion of rock mass as a result of freezing of pore water at sub-zero temperatures, which led to fracture closure, hence reducing tensile stresses around fracture tip (Murton et al. 2006).

Notably, for *elastic-unconfined* conditions within the –2.2 to 22.2 °C temperature range, the lowest tensile stresses (12.4 MPa at –2.2 °C) were generated at fracture tip (Table 2). Because of unconfined, tensile stresses tend to be distributed more broadly within the unconfined rock mass, rather than in confined conditions, hence the smaller tensile stresses generated at the fracture tip.

Table 2. Maximum tensile stress results under elastic analysis.

Temperature range	Elastic analysis	
	Boundary conditions	
	Confined	Unconfined
7.8–32.2 °C	30.8 MPa at 7.8 °C	13.2 MPa at 7.8 °C
–2.2–22.2 °C	29.2 MPa at –2.2 °C	12.4 MPa at –2.2 °C

6.2 Elasto-plastic analysis

To understand the behaviour of chert rock mass, a different constitutive model (elasto-plastic) was used. *Elasto-plastic confined* conditions under the same temperature range as in *elastic* analysis were used. Only confined conditions in which tensile stresses exceeded the tensile strength ($\sigma_x > \sigma_t$) are shown. For brevity, no element failures were observed in unconfined conditions. Remarkably, at minimum temperature 7.8 °C (Fig. 12a), there was tensile failure of 6 elements around the fracture tip. Similarly, for *elasto-plastic confined* conditions at –2.2 °C, tensile failure of 4 elements occurred at the fracture tip (Fig. 12b).

7 Concluding remarks

To get better insight into the causative agents of rock falls, natural rock slope deformation across fractures in a chert rock mass was monitored using six surface fracture displacement sensors, and those arising from thermal stresses were predicted using two-dimensional finite element analysis. Using the new and simple proposed method (Eqns. [1] and [2]), the deformations can be divided into two parts: 1) those proportional to temperature variation, and 2) the other component u' (corrected displacement). By minimizing the first component (due to thermal response), the u' can be well recognized. After thermal correction of field data, under u' , ch1 gave a clear rock mass movement, which could be related to fracture growth (see ch1, Fig. 8). Ch3 and 5, exhibit very small temperature-induced permanent fracture displacements (due to thermal change) over a period of over two years. Ch4 was gradually opening whilst ch6 was generally closing. Insignificant influences of weather conditions on fracture/rock mass movement were observed.

Using numerical analyses, in the rock mass model (Fig. 9), tensile stresses that were large enough to induce fracture growth appeared at the fracture tip when temperature lowered. This research suggests that freezing

effects on deformation of chert rock mass are insignificant, and we tentatively suggest that thermal fatigue predominantly caused the permanent fracture deformations. Further details of numerical analyses are found in Mufundirwa et al. (2011). The yields from this study allow us to expand on our future investigations into the precursors leading to these rock falls.

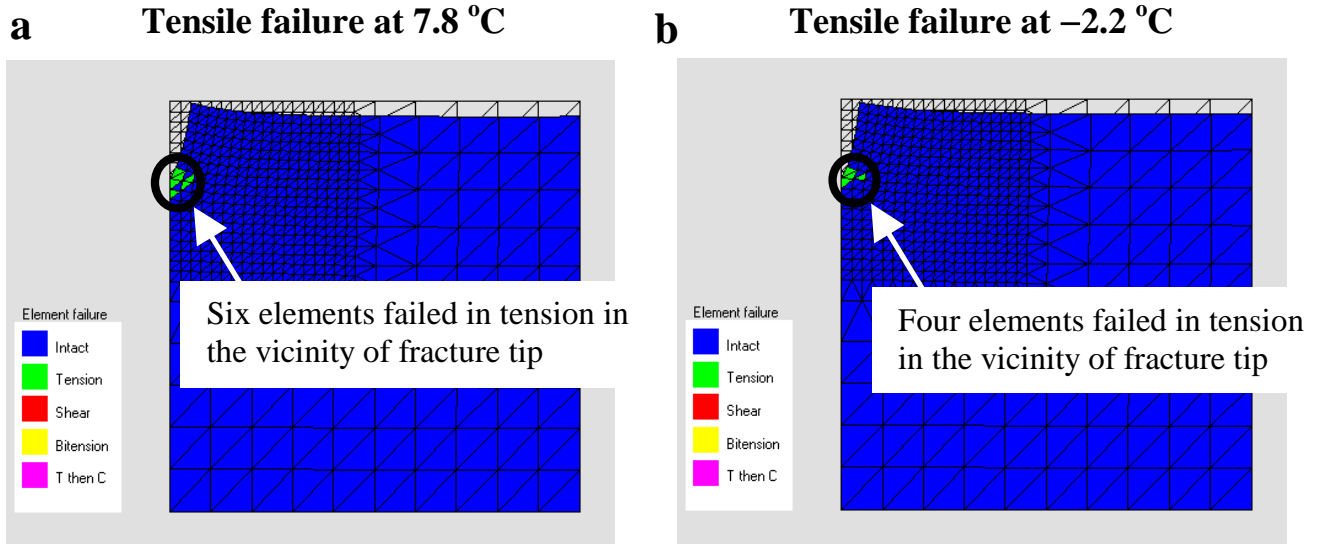


Figure 12. Calculated results of Elasto-plastic confined FE model: (a) Element failure at minimum temperature 7.8 °C and (b) Element failure at minimum temperature -2.2 °C. *Note:* Deformation is magnified $\times 1000$.

8 References

- Crank, J. (1975). *The mathematics of diffusion*. Oxford university press, Oxford, pp. 144–146.
- Ishiguro, S., Nakaya, M. (1986). Temperature distribution analysis of concrete in fill dam gallery. *Bulletin of the University of Osaka Prefecture, Ser. B* 38: 35–43.
- Kostak, B., Dobrev, N., Zika, P., Ivanov, P. (1998). Joint monitoring on a rock face bearing an historical bas-relief. *Quarterly Journal of Engineering Geology and Hydrogeology* 31: 37–45.
- Matsuoka, N. (2001). Direct observation of frost wedging in alpine bedrock. *Earth Surface Processes and Landforms* 26: 601–614.
- Matsuoka, N. (2008). Frost weathering and rockwall erosion in the southeastern Swiss Alps: long-term (1994–2006) observations. *Geomorphology* 99: 353–368.
- Mufundirwa, A., Fujii, Y., Kodama, N., Kodama, J. (2011). Analysis of natural rock slope deformations under temperature variation: A case from a cool temperate region in Japan. *Cold Regions Science and Technology* 65: 488–500.
- Murton, J.B., Peterson, R., Ozouf, J. (2006). Bedrock fracture by ice segregation in cold regions. *Science* 314(5802): 1127–1129.
- Nicholson, D.T., Hencher, S.R. (1997). Assessing the potential for deterioration of engineered rock slopes, in: Marinos, P.G., Koukis, G.C., Tsiambaos, G.C., Stournaras, G.C. (eds.), *Engineering Geology and the Environment*, Balkema, Rotterdam, pp. 911–917.
- Nicholson, D.T., Nicholson, F.H. (2000). Physical deterioration of sedimentary rocks subjected to experimental freeze-thaw weathering. *Earth Surface Processes and Landforms* 25: 1295–1307.
- Saito, M. (1965). Forecasting the time of occurrence of a slope failure. *Proceedings of 6th International Conference on Soil Mechanics and Foundation Engineering, Montreal*, 2, pp. 537–541.
- Saito, M. (1969). Forecasting time of slope failure by tertiary creep. *Proceedings of 7th International Conference on Soil Mechanics and Foundation Engineering, Mexico City*, 2, pp. 677–683.

- Shiotani, T. (2003). Evaluation of rock stability by means of acoustic emission. *International Conference on Emerging Technologies in Non-Destructive Testing, Greece*.
- Waragai, T. (1998). Effects of Rock Surface Temperature on Exfoliation, Rock Varnish, and Lichens on a Boulder in the Hunza Valley, Karakoram Mountains, Pakistan. *Arctic and Alpine Research* 30: 184–192.
- Timoshenko, S.P., Goodier, J.N. (1969). *Theory of elasticity*. McGraw-Hill, New York, 2nd edition.
- William, H.P., Teukolsky, S.A., William, T.V., Brian, P.F. (2007). *Numerical recipes, The art of scientific computing*. Cambridge University Press, New York, pp. 1045–1052.